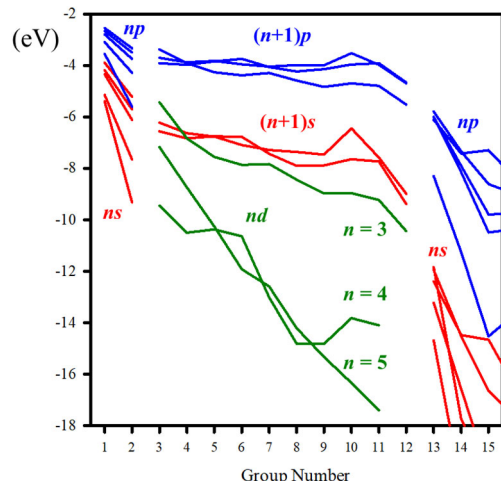


(32) Tight-binding theory considers valence electrons that are more closely held at atoms but become delocalized throughout the solid by valence orbital overlap. The model is appropriate for semiconductors like Si and Ge, insulators and salts such as AlP and NaCl, and *d*-metals and their compounds. In fact, tight-binding theory has significant similarities to *molecular orbital (MO) theory*. Any calculation of electronic structure requires choosing an atomic orbital (AO) basis set, which is frequently a minimal basis set incorporating just valence atomic orbitals. To each of these AOs is assigned a *valence orbital energy*, which can be determined empirically from atomic spectra or from Hartree-Fock calculations, as shown here.<sup>10</sup> These energies reflect trends in atomic electronegativities.



Then, symmetry-adapted-linear-combinations (SALCs) of these AOs are constructed. In MO theory, the SALCs make use of the irreducible representations of the molecular point group; for tight-binding theory, the corresponding SALCs are constructed using the irreducible representations of the subgroup of lattice translations of the space group. With these SALCs, the finite, Hermitian Hamiltonian matrix ( $H$ ) is constructed. In MO theory,  $H$  has dimension equal to the number of basis AOs in the molecule. In tight-binding theory,  $H(\mathbf{k})$  is constructed for appropriately selected wavevectors and has dimension equal to the number of basis AOs in one unit cell. Solving the secular determinant yields for the eigenvalues (electronic energies) and eigenfunctions (AO coefficients). These numerical results are then used to generate relevant information and diagrams. For MO theory, the output includes MO energy diagrams, determining the highest occupied and lowest unoccupied MOs, i.e., the HOMO and LUMO, and performing population analyses with the AO coefficients to obtain electron density distributions and bonding analysis. The results of a tight-binding calculation generate electronic density of states diagrams, which are quasi-continuous distributions of electron energy levels that can be decomposed into partial density of states from various orbital or atomic components, and the corresponding Fermi level, which is the solid-state analogue of the HOMO for a molecule. Population analysis can also be carried out and provides crystal orbital overlap population (COOP) or Hamilton population (COHP) diagrams used for identifying important bonding features. Lastly, *band structure diagrams* or *energy dispersion curves*, which are energies plotted as a function of wavevector  $\mathbf{k}$  along specific directions in wavevector space.

<sup>10</sup> A.Herman, *Modelling Simul. Mater. Sci. Eng.*, **2004**, 12, 21-32.

BRIEF TUTORIAL on Molecular Orbital Theory: MOs are stabilized relative to their constituent AOs when the overlap  $S$  is *in-phase*. Likewise, MOs are destabilized relative to their constituent AOs when the overlap is *out-of-phase*. Interactions between atoms also depend on how the MOs are filled with electrons:

Degenerate Interaction		Nondegenerate Interaction	

Two-center (orbital), two-electron interactions are stabilizing, and they depend on whether the two AOs have the same energy (*degenerate*) or not (*nondegenerate*). The size of the interaction energy  $\Delta E$  increases as the orbital overlap  $S$  increases. Also, two-center, four-electron interactions are destabilizing because the antibonding MO is destabilized more than the bonding MO is stabilized. As the diagram illustrates, the bonding MO for the nondegenerate case has greater AO contribution from the more electronegative (lower energy) AO, and vice versa for the antibonding MO. Although not illustrated here, the magnitudes of AO overlaps generally decrease from  $\sigma$ - to  $\pi$ -type overlap.

**(33)  $\pi$ -Molecular Orbitals of Benzene – an MO treatment:** Before applying tight-binding theory on model and real solids, let's start with a molecular example to introduce the procedures and some important outcomes. The basis set consists of six  $2p_z$  AOs of the six C atoms:  $\{\varphi_{z1}, \varphi_{z2}, \varphi_{z3}, \varphi_{z4}, \varphi_{z5}, \varphi_{z6}\}$ . The point group of benzene is  $D_{6h}$  but we can restrict focus to the rotation group  $C_6 = \{C_6, C_6^2, C_6^3, C_6^4, C_6^5, C_6^6 = E\}$ . Since  $C_6$  is an Abelian group, each operation  $C_6^m$  belongs to its own class and there are six irreducible representations (IRs), which can be assigned using the quantum numbers  $l = 1, 2, 3, 4, 5, 6$ . The character  $\chi_l$  of the  $l^{\text{th}}$  IR for the operation  $C_6^m$  is  $e^{2\pi i l m / 6}$ . By using these characters, the general recipe for writing the six SALCs (one for each IR) is

$$\psi_l = \frac{1}{\sqrt{6}} \sum_{m=1}^6 \chi_l(C_6^m) \varphi_{zm} = \frac{1}{\sqrt{6}} \sum_{m=1}^6 e^{2\pi i l m / 6} \varphi_{zm}.$$

Therefore, the six SALCs for the  $\pi$ -orbitals of benzene are:

$$\begin{aligned} \psi_1 &= \frac{1}{\sqrt{6}} (e^{2\pi i / 6} \varphi_{z1} + e^{4\pi i / 6} \varphi_{z2} + e^{6\pi i / 6} \varphi_{z3} + e^{8\pi i / 6} \varphi_{z4} + e^{10\pi i / 6} \varphi_{z5} + e^{12\pi i / 6} \varphi_{z6}) \\ \psi_2 &= \frac{1}{\sqrt{6}} (e^{4\pi i / 6} \varphi_{z1} + e^{8\pi i / 6} \varphi_{z2} + e^{12\pi i / 6} \varphi_{z3} + e^{16\pi i / 6} \varphi_{z4} + e^{20\pi i / 6} \varphi_{z5} + e^{24\pi i / 6} \varphi_{z6}) \\ \psi_3 &= \frac{1}{\sqrt{6}} (e^{6\pi i / 6} \varphi_{z1} + e^{12\pi i / 6} \varphi_{z2} + e^{18\pi i / 6} \varphi_{z3} + e^{24\pi i / 6} \varphi_{z4} + e^{30\pi i / 6} \varphi_{z5} + e^{36\pi i / 6} \varphi_{z6}) \\ \psi_4 &= \frac{1}{\sqrt{6}} (e^{8\pi i / 6} \varphi_{z1} + e^{16\pi i / 6} \varphi_{z2} + e^{24\pi i / 6} \varphi_{z3} + e^{32\pi i / 6} \varphi_{z4} + e^{40\pi i / 6} \varphi_{z5} + e^{48\pi i / 6} \varphi_{z6}) \\ \psi_5 &= \frac{1}{\sqrt{6}} (e^{10\pi i / 6} \varphi_{z1} + e^{20\pi i / 6} \varphi_{z2} + e^{30\pi i / 6} \varphi_{z3} + e^{40\pi i / 6} \varphi_{z4} + e^{50\pi i / 6} \varphi_{z5} + e^{60\pi i / 6} \varphi_{z6}) \\ \psi_6 &= \frac{1}{\sqrt{6}} (e^{12\pi i / 6} \varphi_{z1} + e^{24\pi i / 6} \varphi_{z2} + e^{36\pi i / 6} \varphi_{z3} + e^{48\pi i / 6} \varphi_{z4} + e^{60\pi i / 6} \varphi_{z5} + e^{72\pi i / 6} \varphi_{z6}) \end{aligned}$$

To construct the Hamiltonian matrix, we need to choose a quantum mechanical method. An especially simple approach, which captures the important symmetry of the problem, is *simple Hückel theory*. For the  $\pi$ -MOs of benzene, the Hamiltonian matrix elements involve two distinct integrals between AOs:

$$\alpha \equiv H_{mm} = \langle \varphi_{zm} | H | \varphi_{zm} \rangle = \int \varphi_{zm}^*(\mathbf{r}) H \varphi_{zm}(\mathbf{r}) d\mathbf{r} = \text{coulomb integral.}$$

These values correspond to the AO energy of  $\varphi_{zm}$  at site  $m$ . For carbon,  $\alpha = -11.4$  eV. However,  $\alpha$  can also serve as a reference energy for the calculation and is often assigned the value 0.

$$\beta \equiv H_{mm'} = \langle \varphi_{zm} | H | \varphi_{zm'} \rangle = \int \varphi_{zm}^*(\mathbf{r}) H \varphi_{zm'}(\mathbf{r}) d\mathbf{r} = \text{resonance integral, or interaction energy between AOs on different sites. For Hückel theory, only AOs on adjacent sites interact, i.e., } m' = m \pm 1, \text{ so there is a single value. For two carbon atoms, the } \pi \text{ resonance integral is } -2.8 \pm 0.3 \text{ eV. In general, } \beta < 0 \text{ to represent a stabilizing interaction.}$$

With these parameters, the Hamiltonian matrix elements  $H_{ll'} = \langle \psi_l | H | \psi_{l'} \rangle$  between SALCs  $\psi_l$  and  $\psi_{l'}$  are:

$$\begin{aligned} H_{ll'} &= \frac{1}{6} \sum_{m=1}^6 \sum_{m'=1}^6 e^{-2\pi i l m / 6} e^{2\pi i l' m' / 6} \langle \varphi_{zm} | H | \varphi_{zm'} \rangle \\ &= \frac{1}{6} \sum_{m=1}^6 (e^{-2\pi i l m / 6} e^{2\pi i l' (m-1) / 6} \beta + e^{-2\pi i l m / 6} e^{2\pi i l' m / 6} \alpha + e^{-2\pi i l m / 6} e^{2\pi i l' (m+1) / 6} \beta) \\ &= \frac{1}{6} \sum_{m=1}^6 e^{2\pi i (l' - l) m / 6} \left( \alpha + 2\beta \cos \frac{2\pi l'}{6} \right) = \left( \alpha + 2\beta \cos \frac{2\pi l'}{6} \right) \delta_{ll'}. \end{aligned}$$

This calculation affirms that the SALCs are eigenfunctions of the Hamiltonian operator. The corresponding eigenvalues (energies) are:

$$E_l = \langle \psi_l | H | \psi_l \rangle = \alpha + 2\beta \cos \frac{2\pi l}{6}.$$

According to this expression,  $E_1 = E_5$ ,  $E_2 = E_4$ ,  $E_3$  is highest (most antibonding), and  $E_6$  is lowest (most bonding). By examining the nodal character of these MOs, the SALCs labeled by  $l = 4, 5, 6$  can be shifted downward by 6, so that the six MO labels (“quantum numbers”) become  $-2, -1, 0, 1, 2, 3$ . As a result,  $|l|$  gives the number of nodes for  $\psi_l$ . The solutions are:

$$l = 0: \quad E_0 = \alpha + 2\beta, \quad \psi_0 = \frac{1}{\sqrt{6}} (\varphi_{z1} + \varphi_{z2} + \varphi_{z3} + \varphi_{z4} + \varphi_{z5} + \varphi_{z6})$$

There are no nodes between AOs on adjacent sites, so the MO is totally bonding.

$$l = 1: \quad E_1 = \alpha + \beta, \quad \psi_1 = \frac{1}{\sqrt{6}} (e^{\pi i / 3} \varphi_{z1} + e^{2\pi i / 3} \varphi_{z2} - \varphi_{z3} + e^{-2\pi i / 3} \varphi_{z4} + e^{-\pi i / 3} \varphi_{z5} + \varphi_{z6})$$

$$l = -1: \quad E_{-1} = \alpha + \beta, \quad \psi_{-1} = \frac{1}{\sqrt{6}} (e^{-\pi i / 3} \varphi_{z1} + e^{-2\pi i / 3} \varphi_{z2} - \varphi_{z3} + e^{2\pi i / 3} \varphi_{z4} + e^{\pi i / 3} \varphi_{z5} + \varphi_{z6})$$

These 2 MOs are complex conjugate functions, which makes them degenerate. They can be transformed into real functions by taking linear combinations as follows:

$$\begin{aligned} \frac{1}{\sqrt{2}} (\psi_1 + \psi_{-1}) &= \frac{1}{\sqrt{12}} (\varphi_{z1} - \varphi_{z2} - 2\varphi_{z3} - \varphi_{z4} + \varphi_{z5} + 2\varphi_{z6}) \\ \frac{1}{\sqrt{2}} (\psi_1 - \psi_{-1}) &= \frac{1}{2} (\varphi_{z1} + \varphi_{z2} - \varphi_{z4} - \varphi_{z5}) \end{aligned}$$

The resulting transformed functions each have 1 node.

$$l = 2: \quad E_2 = \alpha - \beta, \quad \psi_2 = \frac{1}{\sqrt{6}} (e^{2\pi i / 3} \varphi_{z1} + e^{-2\pi i / 3} \varphi_{z2} + \varphi_{z3} + e^{-2\pi i / 3} \varphi_{z4} + e^{2\pi i / 3} \varphi_{z5} + \varphi_{z6})$$

$$l = -2: \quad E_{-2} = \alpha - \beta, \quad \psi_{-2} = \frac{1}{\sqrt{6}}(e^{-2\pi i/3}\varphi_{z1} + e^{2\pi i/3}\varphi_{z2} + \varphi_{z3} + e^{2\pi i/3}\varphi_{z4} + e^{-2\pi i/3}\varphi_{z5} + \varphi_{z6})$$

These 2 MOs are complex conjugate functions, which makes them degenerate. They can be transformed into real functions by taking linear combinations as follows:

$$\begin{aligned} \frac{1}{\sqrt{2}}(\psi_2 + \psi_{-2}) &= \frac{1}{\sqrt{12}}(-\varphi_{z1} - \varphi_{z2} + 2\varphi_{z3} - \varphi_{z4} + \varphi_{z5} + 2\varphi_{z6}) \\ \frac{1}{\sqrt{2}}(\psi_2 - \psi_{-2}) &= \frac{1}{2}(-\varphi_{z1} + \varphi_{z2} - \varphi_{z4} + \varphi_{z5}) \end{aligned}$$

The resulting transformed functions each have 1 node.

$$l = 3: \quad E_3 = \alpha - 2\beta, \quad \psi_3 = \frac{1}{\sqrt{6}}(-\varphi_{z1} + \varphi_{z2} - \varphi_{z3} + \varphi_{z4} - \varphi_{z5} + \varphi_{z6})$$

There are nodes between AOs on adjacent sites, so the MO is totally antibonding.

The *density of states* (DOS)  $n(E)$  diagram plots the number of states within a small energy range  $dE$ . For a molecule, the DOS plot contains delta functions at every MO energy with a height corresponding to the degeneracy  $D_l$  of the MO:  $n(E) = D_l \delta(E - E_l)$ .

An important chemical bonding parameter arising from a population analysis of the MOs is the *overlap population* or *bond index* for a pair of interacting atoms (AOs) for each MO. This numerical index can be positive, negative, or zero, which corresponds, respectively, to *bonding*, *antibonding*, or *nonbonding* interactions. In Hückel theory, the overlap population is the product of AO coefficients on adjacent sites and is summed over all symmetry-equivalent pairs. For the  $\pi$ -MOs of benzene, the C–C overlap population  $p_l$  for MO  $\psi_l$  is:

$$p_l = \frac{1}{6} \sum_{m=1}^6 (e^{-2\pi i l m/6} e^{-2\pi i l (m+1)/6} + e^{-2\pi i l m/6} e^{-2\pi i l (m-1)/6}) = 2 \cos \frac{2\pi l}{6}.$$

In benzene, there are three bonding  $\pi$ -MOs and three antibonding  $\pi$ -MOs. The plot of the overlap populations follows the same energy axis as the MO energy and DOS diagrams.

**(34) Overlap and Hamilton Populations:** These features of an MO or tight-binding calculation on a molecule or solid provide useful information about the nature of interatomic interactions as being net bonding, antibonding, or nonbonding. Therefore, it is useful to understand how these values come about and how they relate to these interactions. So, let's examine them for the H<sub>2</sub> molecule. The two MOs for H<sub>2</sub> are:

$$\text{Bonding MO:} \quad \psi_1(x) = c_{11}\varphi_1\left(x + \frac{d}{2}\right) + c_{12}\varphi_2\left(x - \frac{d}{2}\right)$$

$$\text{Antibonding MO:} \quad \psi_2(x) = c_{21}\varphi_1\left(x + \frac{d}{2}\right) - c_{22}\varphi_2\left(x - \frac{d}{2}\right)$$

In these expressions, the coefficients for the AOs  $\varphi_1$  and  $\varphi_2$  are positive numbers and the nodal characters are explicitly shown by the signs in the linear combinations. The population analysis of each MO is the integral over all space:

$$\text{For the Bonding MO:} \quad 2\langle\psi_1|\psi_1\rangle = 2(c_{11}^2 + c_{12}^2) + 2c_{11}c_{12}S_{12}$$

$$\text{For the Antibonding MO:} \quad 2\langle\psi_2|\psi_2\rangle = 2(c_{21}^2 + c_{22}^2) - 2c_{21}c_{22}S_{12}$$

The terms in red identify the overlap populations for each MO and gives the *number of electrons* assigned to orbital overlap. A positive value means that electron density builds up between the atom pair to establish bonding (attractive) interaction. A negative value means that electron density is depleted between the atom pair to establish an antibonding (repulsive) interaction. By expressing the wavefunctions with respect to an origin halfway between each nucleus, the electron

densities of each MO relative to the sum of the neutral atom AOs can be plotted, which corroborates the population analysis.

Given the basis set dependency of spatial overlap integrals, an alternative population analysis has been worked out using the Hamiltonian:

For the Bonding MO:

$$2\langle\psi_1|H|\psi_1\rangle = 2(c_{11}^2H_{11} + c_{12}^2H_{22}) + 2c_{11}c_{12}H_{12} = 2(c_{11}^2 + c_{12}^2)\epsilon_0 + 2c_{11}c_{12}H_{12}$$

For the Antibonding MO:

$$2\langle\psi_2|H|\psi_2\rangle = 2(c_{21}^2H_{11} + c_{22}^2H_{22}) - 2c_{21}c_{22}H_{12} = 2(c_{21}^2 + c_{22}^2)\epsilon_0 - 2c_{21}c_{22}H_{12}$$

The expressions in red are called the *Hamilton population* and provide an evaluation of the strength (units are energy) of interatomic orbital interactions. Since  $H_{12} < 0$ , a negative Hamilton population signifies a bonding interaction, and a positive Hamilton population signifies an antibonding interaction. Hamilton populations were designed to be applied to programs that utilize density functional theory in which atomic orbital basis sets are not always used. Nonetheless, the Hamilton populations provide similar information as overlap populations from tight-binding theory.

**(35) Energy Band of a 1-d Solid:** The MO energy diagram for the  $\pi$ -MOs of benzene can be plotted as  $E_l$  as a function of the quantum number  $l$ . The six energy values from  $l = -2$  to  $l = 3$  vary according to the cosine relationship worked out above in slide **(31)** and, when plotted in this way, can be called a *band diagram*. The lowest energy MO is totally bonding; the highest energy MO is totally antibonding. In fact, the energy expression yields the same energies for quantum numbers " $l$ " =  $-3$  and  $l = 3$ , but " $l$ " =  $-3$  is not necessary to label the MOs; only a cycle of six consecutive integers is necessary.

**(36)** The problem of the six  $\pi$ -MOs of benzene can be readily extended to a large  $N$ -atom ring composed of  $N$   $p_z$  AOs  $\varphi_z$ :

$$\psi_l = \frac{1}{\sqrt{N}} \sum_{m=1}^N e^{il(m \cdot 2\pi/N)} \varphi_{zm} \text{ with energies } E_l = \alpha + 2\beta \cos \frac{2\pi l}{N}.$$

The MOs are labeled by  $N$  quantum numbers  $l = 1, \dots, N$ , but like benzene, the sequence can be revised to  $l = -\frac{(N-1)}{2}, \dots, 0, \dots, \frac{N}{2}$ .

A 1-d chain of  $p_z$  AOs  $\varphi_z$  can be constructed from this  $N$ -atom ring by severing one of the interatomic connections. Now, instead of a group with  $N$  rotations  $\left\{\frac{2\pi m}{N}, m = 1, \dots, N\right\}$ , we have created a chain with  $N$  translations with length  $a$ . To keep the problem equivalent to the ring, *periodic boundary conditions* are applied, which means that the translation  $Na$ , like the rotation  $N(2\pi/N)$ , is the identity member of the group. Therefore, the group of translations becomes  $\{ma, m = 1, \dots, N\}$ . The associated labels of the IRs are the wavevectors  $k = 2\pi l/Na$  for integers  $l = 1, \dots, N$ . As done for the benzene ring, the integers are shifted to the sequence  $-\frac{(N-1)}{2}, \dots, 0, \dots, \frac{N}{2}$ . As the size of the translation group  $N$  grows, the distance between adjacent wavevectors shrinks, so that we can consider the set of allowed wavevectors to be *quasi-continuous*. As a result of this construction, the allowed wavevectors are  $-\pi/a < k \leq \pi/a$ . Also analogous to the  $\pi$ -MOs of benzene, the wavefunctions and energy values are:

$$\psi_k = \frac{1}{\sqrt{N}} \sum_{m=1}^N e^{ikma} \varphi_{zm} \text{ with energies } E_k = \alpha + 2\beta \cos ka.$$

(37) *Bloch's Theorem* is an important statement of the behavior of electronic wavefunctions in a crystal, in which the potential felt by an electron is periodic and has the full periodicity of the lattice  $V(\mathbf{r} + \mathbf{T}) = V(\mathbf{r})$ . Bloch's theorem states that the electronic wavefunctions  $\psi_{nk}$  subjected to such a periodic potential take the form

$$\psi_{nk}(\mathbf{r}) = e^{i\mathbf{k}\cdot\mathbf{r}} u_{nk}(\mathbf{r}),$$

in which  $u_{nk}(\mathbf{r})$  is totally symmetric for the lattice, i.e.,  $u_{nk}(\mathbf{r} + \mathbf{T}) = u_{nk}(\mathbf{r})$ . In other words, Bloch wavefunctions are essentially plane waves with amplitudes that are periodic in the lattice of the crystal. The labels of each wavefunction are the wavevector  $\mathbf{k}$ , which provides nodal information with respect to lattice translations, and the quantum number  $n$ , which can identify the nature of the basis functions making up the Bloch wavefunction, such as  $s, p, d$  AOs. There are three important ramifications of Bloch's theorem:

- (1) A Bloch wavefunction evaluated at a position shifted by a lattice vector is related the value of the Bloch wavefunction at the original position by a phase factor:

$$\psi_{nk}(\mathbf{r} + \mathbf{T}) = e^{i\mathbf{k}\cdot(\mathbf{r}+\mathbf{T})} u_{nk}(\mathbf{r} + \mathbf{T}) = e^{i\mathbf{k}\cdot\mathbf{T}} e^{i\mathbf{k}\cdot\mathbf{r}} u_{nk}(\mathbf{r}) = e^{i\mathbf{k}\cdot\mathbf{T}} \psi_{nk}(\mathbf{r}).$$

This is an extremely valuable result because if the wavefunction is known in one unit cell, the wavefunction can be evaluated in *any other unit cell* of the crystals.

- (2) If  $\mathbf{K}$  is a reciprocal lattice vector, then two Bloch wavefunctions  $\psi_{nk}$  and  $\psi_{n(\mathbf{k}+\mathbf{K})}$  for the different wavevectors  $\mathbf{k}$  and  $\mathbf{k} + \mathbf{K}$  are basis functions for the same IR of the group of lattice translations, i.e., they have the same symmetry properties with respect to lattice periodicity:

$$\psi_{nk}(\mathbf{r} + \mathbf{T}) = e^{i\mathbf{k}\cdot\mathbf{T}} \psi_{nk}(\mathbf{r}),$$

$$\psi_{n(\mathbf{k}+\mathbf{K})}(\mathbf{r} + \mathbf{T}) = e^{i(\mathbf{k}+\mathbf{K})\cdot\mathbf{T}} \psi_{n(\mathbf{k}+\mathbf{K})}(\mathbf{r}) = e^{i\mathbf{k}\cdot\mathbf{T}} e^{i\mathbf{K}\cdot\mathbf{T}} \psi_{n(\mathbf{k}+\mathbf{K})}(\mathbf{r}) = e^{i\mathbf{k}\cdot\mathbf{T}} \psi_{n(\mathbf{k}+\mathbf{K})}(\mathbf{r}).$$

The second equation occurs because  $\mathbf{K} \cdot \mathbf{T} = 2\pi N$ , so that  $e^{i\mathbf{K}\cdot\mathbf{T}} = 1$ . Both wavefunctions  $\psi_{nk}$  and  $\psi_{n(\mathbf{k}+\mathbf{K})}$  show the same phase factor for the same lattice translation, i.e., these two wavefunctions have identical symmetry properties. Therefore, along a specific direction in reciprocal space, the allowed wavevectors can be  $\mathbf{0} \leq \mathbf{k} < \mathbf{K}$ , but it the preferred choice is  $-\mathbf{K}/2 < \mathbf{k} \leq \mathbf{K}/2$  with the reciprocal lattice point  $\mathbf{K} = \mathbf{0}$  in the middle. This region is called the *first Brillouin zone*. The point  $\mathbf{K} = \mathbf{0}$  is called the zone center and designated  $\Gamma$ ; the point  $\mathbf{K}/2$  is on the Brillouin zone *boundary* and receives various designations depending on the lattice symmetry. For a 1-d lattice, the range of allowed wavevectors is restricted to  $0 \leq k < 2\pi/a$ , and the first Brillouin zone becomes  $-\pi/a < k \leq \pi/a$ .

- (3) The Bloch wavefunction  $\psi_{n(-\mathbf{k})}$  is the complex conjugate of  $\psi_{nk}$ :

$$\psi_{n(-\mathbf{k})}(\mathbf{r}) = e^{-i\mathbf{k}\cdot\mathbf{r}} u_{n(-\mathbf{k})}(\mathbf{r}) = e^{-i\mathbf{k}\cdot\mathbf{r}} u_{nk}^*(\mathbf{r}) = [e^{i\mathbf{k}\cdot\mathbf{r}} u_{nk}(\mathbf{r})]^* = \psi_{nk}^*(\mathbf{r})$$

which is true as long as  $u_{n(-\mathbf{k})}(\mathbf{r}) = u_{nk}^*(\mathbf{r})$ . For Schrödinger's equation of a static lattice and no applied fields, this relationship between the amplitude functions holds. As a result, the energies corresponding to  $\psi_{n(-\mathbf{k})}$  and  $\psi_{nk}$  are equal, i.e.,  $E_{-\mathbf{k}} = E_{\mathbf{k}}$  and these two wavefunctions are degenerate. Therefore, for electronic structure calculations, the region of reciprocal space used for selected  $\mathbf{k}$ -points can be modified to  $\mathbf{0} \leq \mathbf{k} \leq \mathbf{K}/2$ , which is called the *irreducible wedge* of the Brillouin zone.

When doing electronic structure calculations on crystals, several  $\mathbf{k}$ -points are selected from the boundaries and interior of the irreducible wedge of the Brillouin zone. For each wavevector, the Hamiltonian matrix is constructed and solved for its eigenvalues (energies) and eigenfunctions (coefficients of the basis functions). From these results, energy band structures, density of states, and crystal orbital overlap population (COOP) or crystal orbital Hamilton population (COHP) curves are determined for bonding analysis.

**(38) Brillouin Zones:** The first Brillouin zone is the Wigner-Seitz cell surrounding a reciprocal lattice point, which is designated as the  $\Gamma$  point (0,0,0).

- For a 1-d real space lattice with lattice constant  $a$ , the 1-d reciprocal lattice has lattice constant  $2\pi/a$ . The first Brillouin zone is  $-\pi/a < k \leq \pi/a$ , and the irreducible wedge is  $0 \leq k \leq \pi/a$ , or  $0 \leq k \leq 1/2$  in units of  $2\pi/a$ . The boundary  $k$ -point can be designated X.
- For a 2-d real space lattice with lattice vectors  $\mathbf{a}_1$  and  $\mathbf{a}_2$ , the 2-d reciprocal lattice has a unit cell with  $\mathbf{a}_1^*$  directed perpendicular to  $\mathbf{a}_2$  and length so that  $\mathbf{a}_1 \cdot \mathbf{a}_1^* = 2\pi$ . Likewise,  $\mathbf{a}_2^*$  is directed perpendicular to  $\mathbf{a}_1$  and length so that  $\mathbf{a}_2 \cdot \mathbf{a}_2^* = 2\pi$ . The first Brillouin zone is the region of wavevectors  $(k_1, k_2)$  that is closest to the reciprocal lattice point (0,0). For a hexagonal real space lattice, the Brillouin zone is a hexagonal region surrounding a reciprocal lattice point. The corresponding irreducible wedge is a triangle with an area that is 1/12 of the hexagon. Important boundary points include M = (1/2, 0) and K = (1/3, 1/3). Directions in reciprocal space correspond exactly to directions in real space – this concept is important when considering wavefunctions (crystal orbitals) in crystalline solids.
- For a 3-d real space lattice, the corresponding reciprocal lattice is constructed using the same guidelines mentioned for a 2-d lattice. For electronic structure calculations, using the primitive unit cell  $\mathbf{a}_1, \mathbf{a}_2, \mathbf{a}_3$  is preferred. Then, the reciprocal lattice vectors are:

$$\mathbf{a}_1^* = \frac{2\pi}{V_1} (\mathbf{a}_2 \times \mathbf{a}_3), \quad \mathbf{a}_2^* = \frac{2\pi}{V_1} (\mathbf{a}_3 \times \mathbf{a}_1), \quad \mathbf{a}_3^* = \frac{2\pi}{V_1} (\mathbf{a}_1 \times \mathbf{a}_2),$$

in which  $V_1$  = volume of the primitive unit cell. Some important Brillouin zones for cubic and hexagonal lattices are illustrated.

**(39) A 1-d chain of  $s$  AOs** each separated by distance  $a$  is the simplest model for an extended solid. Periodic boundary conditions treat this chain as a huge ring ( $N \sim 10^8$  atoms). The SALCs are *Bloch wavefunctions* labeled by wavevector  $k$  for  $0 \leq k \leq \pi/a$ :

$$\psi_{sk}(x) = \frac{1}{\sqrt{N}} \sum_{m=1}^N e^{ikma} \varphi_s(x - ma).$$

The wavevector identifies the periodicity of the wavefunction:

$$k = 0: \psi_{sk}(x) = \frac{1}{\sqrt{N}} \sum_m e^0 \varphi_s(x - ma) = \frac{1}{\sqrt{N}} [\varphi_s(x) + \varphi_s(x - a) + \varphi_s(x - 2a) + \varphi_s(x - 3a) + \dots]$$

This wavefunction has the *complete translational symmetry* of the structure because there is *no phase change* in the wavefunction from one unit cell to the next. The de Broglie wavelength  $\lambda = 2\pi/k$  is  $\infty$  for this wavefunction. Moreover, the overlap of adjacent  $s$  AOs is bonding, so this SALC is totally bonding and represents the lowest energy of the band.

$$k = \pi/2a: \psi_{sk}(x) = \frac{1}{\sqrt{N}} \sum_m i^m \varphi_s(x - ma) = \frac{1}{\sqrt{N}} [\varphi_s(x) + i\varphi_s(x - a) - \varphi_s(x - 2a) - i\varphi_s(x - 3a) + \dots]$$

This wavefunction is a complex function. If just the *real* part or just the *imaginary* part is examined, the de Broglie wavelength is  $4a$ . Also, for these two function components, nodes intersect alternant atomic sites, so that this SALC is nonbonding.

$$k = \pi/a: \psi_{sk}(x) = \frac{1}{\sqrt{N}} \sum_m (-1)^m \varphi_s(x - ma) = \frac{1}{\sqrt{N}} [\varphi_s(x) - \varphi_s(x - a) + \varphi_s(x - 2a) - \varphi_s(x - 3a) + \dots]$$

This wavefunction is a real function and represents the shortest wavelength allowed for the lattice; the de Broglie wavelength is  $2a$ . Because adjacent AOs are out-of-phase, this wavefunction is totally antibonding and has the highest energy of the band.

Since two different wavevectors  $k$  and  $k'$  are labels for different IRs of the group of lattice translations, two Bloch wavefunctions  $\psi_{sk}$  and  $\psi_{sk'}$  are *orthogonal* to each other unless  $k' - k$  is a reciprocal lattice vector  $K$ :

$$\langle \psi_{sk}(x) | \psi_{sk'}(x) \rangle = \frac{1}{N} \sum_{m=1}^N \sum_{m'=1}^N e^{i(k'm' - km)a} \langle \varphi_s(x - ma) | \varphi_s(x - m'a) \rangle = \delta(k' - k + K).$$

Therefore, each Bloch wavefunction is an eigenfunction of the Hamiltonian and the corresponding eigenvalue is the energy:

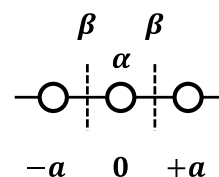
$$E_k = \langle \psi_{sk}(x) | H | \psi_{sk}(x) \rangle = \frac{1}{N} \sum_{m=1}^N \sum_{m'=1}^N e^{ik(m' - m)a} \langle \varphi_s(x - ma) | H | \varphi_s(x - m'a) \rangle$$

Since  $k$  is quasi-continuous, the *band energy*  $E_k$  is also quasi-continuous. Using the Hückel approximation, which includes just nearest neighbor interactions, the energy of the  $s$ -band is:

$$E_k = \frac{1}{N} \sum_{m=1}^N (e^{-ika} \beta + \alpha + e^{ika} \beta) = \frac{1}{N} (N e^{-ika} \beta + N \alpha + N e^{ika} \beta) = \alpha + 2\beta \cos ka.$$

Another way to obtain this expression quickly is to focus on the contents of one unit cell. With one  $s$  AO per unit cell, the Hamiltonian matrix is a  $1 \times 1$  matrix. Inside the unit cell, the energy contribution is  $\alpha$ ; between unit cells, the interaction is  $\beta$  times a phase factor containing the wavevector  $k$  and the lattice translation  $T$ :  $\beta e^{ikT}$ . Using this prescription:

$$\begin{aligned} H_{11} &= \alpha + \beta e^{ik(a)} + \beta e^{ik(-a)} = \alpha + \beta e^{ika} + \beta e^{-ika} \\ &= \alpha + 2\beta \cos ka = E_k. \end{aligned}$$



(40) The important outcomes of a tight-binding calculation include:

- *Band Structure (Dispersion) curves* are plotted as  $E_k$  vs.  $k$  for the wavevector ranging from  $k = 0$  (the Brillouin zone center  $\Gamma$ ) to  $k = \pi/a$  (the Brillouin zone boundary  $X$ ). The energy of the band increases as  $k$  increases. The *band center* is  $\alpha$  for wavevector  $\pi/2a$ . The *bandwidth* is the energy difference between the top and bottom of the band and is  $4\beta$  in this case. Therefore, the bandwidth depends on the strength of the orbital interaction between atomic sites. Like the free-electron model, the Fermi level is controlled by the number of electrons in the band. If there are  $N_e$  electrons per atom/orbital, then  $N_e = 2k_F/(\pi/a) = 2ak_F/\pi$ . The factor 2 arises because each state can hold up to 2 electrons (spin-up and spin-down),  $k_F$  is the Fermi wavevector, and the entire range of states is  $\pi/a$ . For the  $s$ -band,  $0 \leq N_e \leq 2$ . If the chain consists of H atoms, each of which has 1 electron, then the Fermi wavevector is  $\pi/2a$  and the band is *half-filled*. Therefore, certain important quantities that can be evaluated from the band structure based upon the number of electrons  $N_e$  include:

$$\text{Fermi wavevector: } k_F = \frac{\pi N_e}{2a}$$

$$\text{Fermi energy (level): } E_F = \alpha + 2\beta \cos k_F a = \alpha + 2\beta \cos \frac{\pi N_e}{2}$$

$$\begin{aligned} \text{Average band energy: } \langle E_k \rangle &= \frac{2\pi}{a} \int_0^{k_F} (\alpha + 2\beta \cos ka) dk = \frac{2ak_F}{\pi} \left( \alpha + \frac{2\beta}{ak_F} \sin k_F a \right) \\ &= N_e \left( \alpha + \frac{4\beta}{\pi N_e} \sin \frac{\pi N_e}{2} \right) \end{aligned}$$

- *Density of States (DOS) curves* show the number of states in a small energy range  $\Delta E$  over the entire range of energies of the band structure. From the band structure curve  $E_k$  vs.  $k$ , if the same energy window  $\Delta E_k$  is taken at different parts of the band, then the range of wavevectors  $\Delta k$  is larger near the bottom or top of the band, whereas it is smaller near the middle of the band. Therefore, the DOS for the 1-d chain of  $s$  AOs has maximum values near the top and bottom of the band and a minimum at the band center. In other words, the DOS is inversely proportional to the slope of the dispersion curve:

$$\text{DOS} \equiv n(E) \propto \left( \frac{dE}{dk} \right)^{-1} = (2\beta a \sin ka)^{-1}.$$

- *Crystal Orbital Overlap Population (COOP) curves* illustrate interatomic orbital interactions as a function of energy. For the 1-d chain of  $s$  AOs, it is determined by adding up the product of the AO coefficients from adjacent orbitals in the chain:

$$\text{COOP}_k = \frac{1}{N} \sum_{m=1}^N e^{-ikma} (e^{ik(m-1)a} + e^{ik(m+1)a}) = \frac{1}{N} \sum_{m=1}^N (e^{-ika} + e^{ika}) = 2 \cos ka.$$

If  $\text{COOP}_k > 0$ , the state  $k$  is bonding; if  $\text{COOP}_k = 0$ , the state  $k$  is nonbonding; if  $\text{COOP}_k < 0$ , the state  $k$  is antibonding.

**(41)** A 1-d chain of  $p$  AOs demonstrates how band dispersion is related to the symmetry of the AO. For the three different  $p$  AOs, i.e.,  $p_x, p_y, p_z$ , interatomic overlap along the chain involves one  $\sigma$ -type and two orthogonal  $\pi$ -type interactions. Because  $p$  AOs are antisymmetric with respect to inversion, the  $p\sigma$ -band dispersion decreases in energy from the zone center  $\Gamma$  to the zone boundary  $X$ . On the other hand, the dispersion of the two degenerate  $p\pi$ -bands increases in energy from  $\Gamma$  to  $X$ . Since the  $p$  AOs are mutually orthogonal functions, their bands intersect (cross) each other – they are called *symmetry-allowed band crossings*. The bandwidths, which are  $4\beta_\sigma$  and  $4\beta_\pi$ , depend on the orbital overlap and generally increase from  $\pi$ -type to  $\sigma$ -type interactions. The corresponding DOS curve combines the different bands and shows 4 distinct peaks; the COOP curve also combines the individual COOP curves from the different AOs.

**(42)** *Hybridization*: The position of an energy band depends on the AO energy from which it arises. For a main group element with valence  $s$  and  $p$  AOs, the energy of the  $s$ -band will be lower than the energy of the  $p$ -band. With respect to symmetry characteristics, an  $s$  orbital is *even (gerade)* with respect to inversion; the  $p$  orbitals are *odd (ungerade)* with respect to inversion. For the 1-d model, inversion is a symmetry of the chain of atoms. Now, along the  $\Gamma$ - $X$  line in reciprocal space, inversion is a symmetry operation *only* for  $k = 0$  and  $k = \pi/a$ . To see this outcome, operate on different wavevectors with inversion, i.e., evaluate  $i(k) = -k$ :

- $i(0) = -0 = 0$ . The zone center has inversion symmetry.

- (ii)  $i(\pi/a) = -\pi/a$ . The two wavevectors differ by  $2\pi/a$ , which is a reciprocal lattice vector. Since these wavevectors have identical symmetry characteristics, the zone boundary has inversion symmetry.
- (iii)  $i(k) = -k$ . For any wavevector  $0 < k < \pi/a$ ,  $k$  and  $-k$  differ by a length smaller than a reciprocal lattice vector and are not equivalent. Therefore, any general wavevector does not have inversion symmetry.

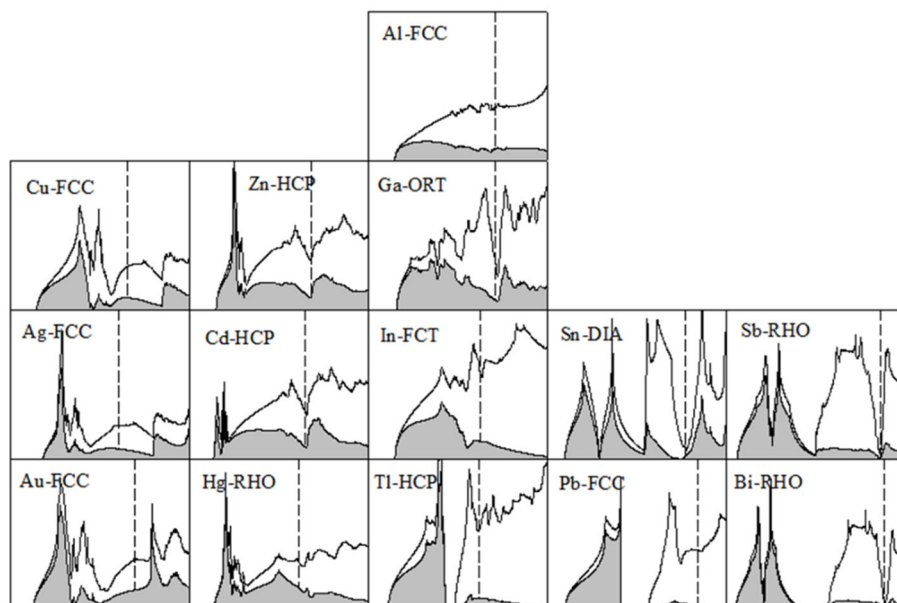
As a result of the symmetry characteristics of the wavevectors and the valence  $s$  and  $p$  AOs, the energy bands at the zone center and boundary are distinctly  $s$ - or  $p$ -type. For any intermediate  $k$ -point  $0 < k < \pi/a$ ,  $s$  and  $p_\sigma$  AOs hybridize, i.e., these functions mix by symmetry, and their energy bands *may not cross* each other along the  $k$ -point line. If the energy difference between  $s$  and  $p$  AOs is large, then the amount of hybridization will be small, and the bands will not cross. However, if this energy difference is small, then these bands will *apparently* cross – an *avoided crossing* occurs. At the zone boundary, the lower energy orbital is  $p_\sigma$ -type and the higher energy orbital is  $s$ -type. The degenerate  $p_\pi$ -bands remain unaffected.

To determine the different band structures, the Hamiltonian matrix is constructed. This matrix is a  $4 \times 4$  matrix because there are 4 AOs in one unit cell:  $s, p_x, p_y, p_z$ :

$$H(k) = \begin{pmatrix} \alpha_s + 2\beta_{s\sigma} \cos ka & -2i\beta_{sp} \sin ka & 0 & 0 \\ 2i\beta_{sp} \sin ka & \alpha_p + 2\beta_{p\sigma} \cos ka & 0 & 0 \\ 0 & 0 & \alpha_p + 2\beta_{p\pi} \cos ka & 0 \\ 0 & 0 & 0 & \alpha_p + 2\beta_{p\pi} \cos ka \end{pmatrix}.$$

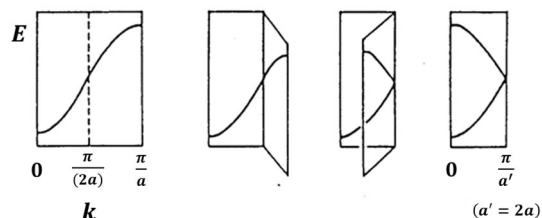
In the  $H(k)$  matrix, the resonance integrals  $\beta$  are negative values. The different signs of the off-diagonal terms  $H_{12}(k)$  and  $H_{21}(k)$  result from the signs of the lobes of the  $p_\sigma$ -AO overlapping with the  $s$ -AO. All other off-diagonal Hamiltonian matrix elements are 0 because they are mutually orthogonal. In general, off-diagonal terms in the Hamiltonian matrix signify orbital overlap between interacting atoms. *Hybridization* is a form of orbital overlap, but it is better defined as mixing of AOs on a single atomic site to represent the geometry of the interatomic bonding, such as the tetrahedrally oriented  $sp^3$  hybrid orbitals at C atoms in methane or diamond. Thus, energy gaps can arise in energy band structures from relative energies of the AO basis functions that overlap with each other or from the hybridization on atomic sites.

Hybridization (or lack thereof) between valence  $s$  and  $p$  AOs can have significant effects on the electronic DOS curves and corresponding structures of the main group metals from Groups 11-15. The DOS curves of the valence  $s$  and  $p$  bands of these metals (shaded regions are  $s$ -bands) show decreasing  $s$ - $p$  hybridization as effective nuclear charge (horizontal) and relativistic effects (vertical) increase. Cu, Ag, Au and Al behave as (nearly) free electron metals, although effects of valence  $d$  AOs are evident for the noble metals. Zn, Cd, In, Tl, and especially Ga, Sb, and Bi have *pseudogaps* in the DOS curve at the Fermi level (a pseudogap is a deep minimum in the DOS curve without creating an actual bandgap); Sb and Bi are called semi-metals. Tl, Pb and Bi show the relativistic effect on electrons in the  $6s$  AOs because these bands are split from the  $6p$  bands.



**(43) Peierls Distortion** (READING: J.K. Burdett, *Chemical Bonding in Solids*, Ch. 2): An important feature of 1-d structures is a Peierls distortion, which is exhibited by a change in bond distances along the chain from equal separations to alternating ...short-long... and occurs for the half-filled band. To demonstrate how this occurs in the electronic structure, consider a 1-d periodic chain of H atoms with repeat distance  $a$ . The energy band is formed by valence  $1s$  AOs and it is half-filled. The band structure, DOS curve, and COOP curve were evaluated in slide (40). For this problem, choose a *doubled* unit cell with two H atoms and repeat distance  $a' = 2a$ . For this setting, there are two orbitals for each  $k$ -point, derived from the bonding and antibonding combinations of the two  $1s$  AOs in the cell. The reciprocal lattice vector now has length  $2\pi/a' = 2\pi/(2a) = \pi/a$ , and the irreducible wedge of the first Brillouin zone becomes  $0 \leq k \leq \pi/a'$  or  $0 \leq k \leq \pi/2a$ . At the zone center ( $\Gamma = 0$ ), the two orbitals are totally bonding and totally antibonding. At the zone boundary ( $k = \pi/a'$ ), with equal H–H distances along the chain, the two bands are net nonbonding and degenerate. The construction of the doubled unit cell creates a glide plane/screw axis as a new symmetry operation of the atomic structure because it transforms one H atom into the other in the unit cell without changing the overall structure of the chain. The presence of this *nonsymmorphic* symmetry operation is responsible for the degeneracy at the zone boundary in the Brillouin zone. This picture is also valid for a planar zig-zag chain of H atoms, for which the unit cell *must* contain two H atoms. Drawing out the crystal orbitals at the zone center and boundary using Bloch's theorem confirm the energies.

Another interpretation of this revised band structure for the doubled unit cell is via *band folding*, as illustrated here. Doubling the size of the real-space unit cell *halves* the size of the reciprocal-space unit cell. For the 1-d chain, the energy band(s) for wavevectors in the range  $\pi/2a < k < \pi/a$  become *folded* back into the region  $0 < k < \pi/2a$ .



Now, consider a distortion in which the two H atoms within each unit cell move closer together, e.g.,  $a - \Delta a$ , so that adjacent H atoms between

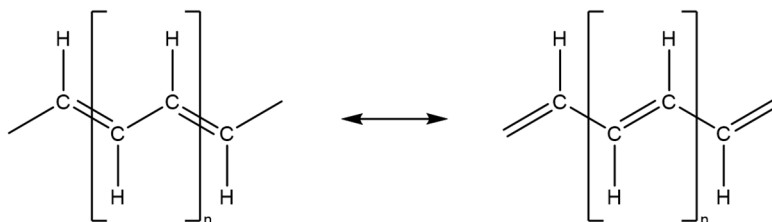
unit cells must increase to  $a + \Delta a$ . From the pictures of the crystal orbitals, the degeneracy at the zone boundary wavevector will be broken: one orbital goes down in energy while the other goes up in energy, and an *energy gap opens at the Fermi level* for the H-atom chain. In other words, a metallic 1-d chain with uniform interatomic distances becomes semiconducting or insulating, depending on the size of the band gap, for the half-filled band case as the interatomic distances alternate ...short-long... along the chain. This demonstrates how a *Peierls distortion* arises. For this model, the revised  $2 \times 2$  Hamiltonian matrix and the eigenvalues for the general model are:

$$H(k) = \begin{pmatrix} \alpha & \beta_1 + \beta_2 e^{ik(-2a)} \\ \beta_1 + \beta_2 e^{ik(2a)} & \alpha \end{pmatrix}; \quad E_k = \alpha \pm [\beta_1^2 + \beta_2^2 + 2\beta_1\beta_2 \cos 2ka]^{1/2}.$$

The energy gap at the zone boundary is a direct measure of the difference between the two different resonance integrals:  $E_{\pi/2a} = \alpha \pm |\beta_1 - \beta_2|$ ;  $E_{\text{gap}} = 2|\beta_1 - \beta_2|$ . In the band structure for the distorted H-atom chain, the greatest changes to the energy bands occur closest to the Fermi level. Therefore, the *driving force* for the distortion is closely related to the position of the Fermi level, which is controlled by the number of valence electrons filling the band structure.

The DOS curve clearly illustrates the band gap. The bands above and below the gap retain the two-peaked character of 1-d systems. The COOP curves can be evaluated for the two different bonds along the chain. The shorter bonds have only bonding character in the lower band and only antibonding character in the higher band. However, the longer bonds of the chain show antibonding character for states below the gap and bonding character for states above the gap.

A classic example of a system showing a Peierls distortion is polyacetylene  $[\text{CH}]_\infty$ , in which the local structure is a planar, zigzag chain of CH groups. The 1-d unit cell contains one acetylene unit which forms C–C bonds to build the polymer. Two Lewis structures for the polymer chain for the case when all C–C distances along the chain have equal weight are:

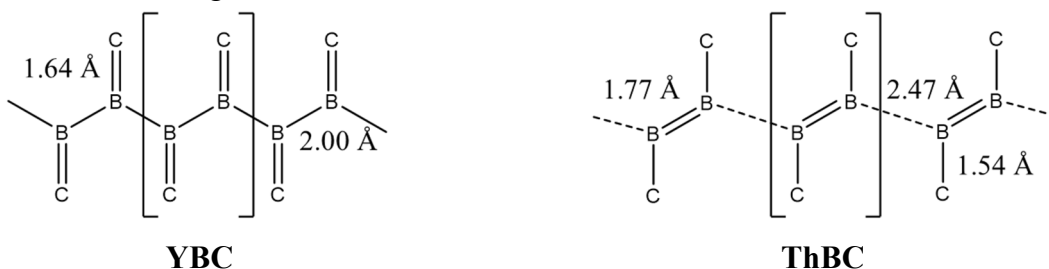


Each C atom is  $sp^2$  hybridized, which provides the  $\sigma$ -bonding backbone; the remaining  $p_z$ -AO is involved in C–C  $\pi$ -bonding along the chain. The band structure of this  $\pi$ -band resembles the picture of the 1s-band for the H-atom chain; each  $p_\pi$ -AO contains 1 valence electron, so the  $\pi$ -band is half-filled. For the chain of equidistant C–C bonds, metallic behavior is expected because there is no energy gap at the Fermi level. But, polyacetylene is a semiconductor, which can be explained by a Peierls distortion because a band gap opens at the Brillouin zone boundary as the C–C distances alternate along the chain. When doped with a small amount of bromine, the carbon-based polymer  $[\text{CH}]\text{Br}_x$  becomes metallic because it has been oxidized, which removes some valence electrons from the  $\pi$ -band, moves the Fermi level away from the degeneracy, and reduces or even eliminates the driving force to distort the chain of C atoms.

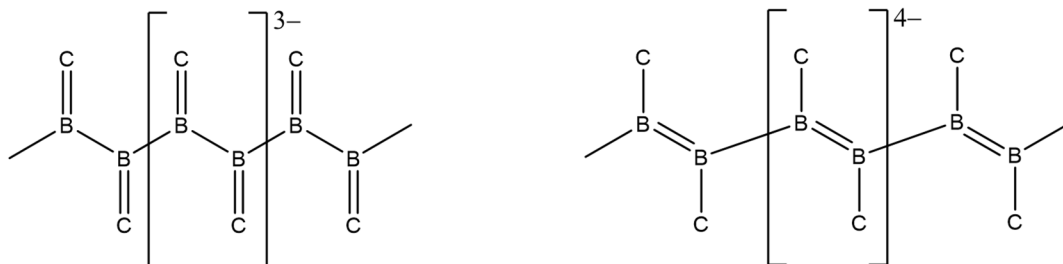
In summary, a Peierls distortion manifests in the electronic structure by energy changes of levels near the half-filled band arising from bond alternation along a 1-d chain. If the chain is oxidized or, equivalently, reduced to change the extent of band filling significantly away from the half-filled band, then the driving force for distortion is small, and the chain will remain undistorted and metallic. Since a Peierls distortion is closely tied to the Fermi level in a 1-d structure,

increasing pressure and temperature can eliminate the occurrence of this type of distortion. Applying pressure usually does not affect nearest neighbor distances but, rather, secondary contacts. As a result, increasing pressure usually promotes interactions between chains, interactions that will shift the position of the Fermi level in the band structure for each 1-d component. Increasing temperature also affects band filling because electrons follow Fermi-Dirac statistics in how they occupy allowed energy states for a structure arising from the Pauli exclusion principle.

(44) Another example of the occurrence of a Peierls distortion can be seen by comparing the structures of the borocarbides YBC and ThBC. YBC and ThBC contain planar  $([BC]^{n-})_{\infty}$  chains which resemble, respectively, undistorted and distorted polyacetylene by forming zigzag chains of B atoms terminated by C atoms. In YBC, the B–B distances are uniform along the chain; in ThBC, they alternate ...short-long... :



Y is *trivalent*, so that YBC has 10 valence electrons per formula unit or 20 valence electrons per unit cell of the chain. On the other hand, Th is *tetravalent*, so that ThBC has 11 valence electrons per formula unit or 22 valence electrons per unit cell of the chain. The following Lewis structures can be constructed for these two structures by obeying the octet rule at B and C atoms:



The calculated band structure and DOS curve for the borocarbide chain with equal B–B distances, as in YBC, is susceptible towards a Peierls distortion for  $[BC]^{4-}$ , as in ThBC, because the Fermi level falls at the degeneracy of the 3<sup>rd</sup> and 4<sup>th</sup>  $\pi$ -band. Within the tight-binding theory, the unit cell contains 16 valence AOs because each atom has 4 *s* and *p* AOs. The band structure curve illustrates 10 bands; there are 2 bands richer in C 2*s* contributions below the energy scale of the band structure and there are 4 bands that are predominantly B–C  $\sigma^*$  orbitals above the energy scale. Among these 10 bands, we can concentrate on the four  $\pi$ -bands: since C is more electronegative than B, the two lower energy bands have greater C character and are B–C bonding, whereas the two higher energy bands have greater B character and are B–C antibonding. Since the chain propagates through B–B interactions, the B–C  $\pi$ -antibonding bands have a larger dispersion (greater bandwidth) than the B–C  $\pi$ -bonding bands.

(45)  $NbI_4$  is a chain of *trans*-edge sharing  $[NbI_2I_{4/2}]$  octahedra. At ambient pressure, the chain is distorted to give alternating ...short-long... Nb–Nb distances:

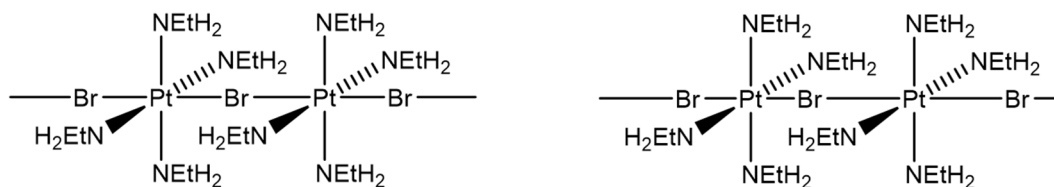


To address the band structure of this compound, we need to identify the position of the Fermi level.  $\text{NbI}_4$  has 33 valence electrons distributed among the four 5s and 5p valence AOs of I and five 4d AOs of Nb. Since I is more electronegative than Nb, the 16 valence AOs of I are lower in energy than the Nb 4d AOs. There are 16 Nb–I bonding and nonbonding (lone pair) orbitals. In the local octahedral ligand field, the Nb 4d AOs will be split into 3 Nb–I  $\pi$ -antibonding  $t_{2g}$  orbitals and 2 Nb–I  $\sigma$ -antibonding  $e_g$  orbitals. Therefore, one valence electron occupies the bands derived from the  $t_{2g}$  orbitals.

Since the distorted structure contains 2  $[\text{NbI}_4]$  formula units per unit cell, there are 6  $t_{2g}$ -derived bands, which meet at degenerate pairs at the Brillouin zone boundary for the band structure of the undistorted  $\text{NbI}_4$  chain. The 3  $t_{2g}$  orbitals are distinguished by the type of metal-metal overlap along the chain: they are  $\sigma$ -,  $\pi$ -, and  $\delta$ -type. The Nb–Nb  $\sigma$ -band is somewhat lower in energy than the others, an effect that is due to the Nb–I orbital interactions. As a result, the Fermi level falls at the degeneracy at the zone boundary of the  $\sigma$ -band. Therefore,  $\text{NbI}_4$  is susceptible to a Peierls distortion.

Another related example showing a Peierls-type distortion is  $\text{VO}_2$ , which undergoes a metal-nonmetal transition as its structure changes from high-temperature, tetragonal rutile-type to a low-temperature, monoclinic structure. Chains of octahedrally coordinated V atoms have uniform V...V distances along the  $c$ -axis in the rutile-type but change to alternating ...short-long... V...V distances in the low-temperature form. Although O atoms bridge neighboring chains, which makes a 3-d structure for  $\text{VO}_2$ , inter-chain interactions are sufficiently weak to allow the Peierls-type metal-metal bond alternation to proceed.

**(46) Charge-Density-Waves (CDWs):** Another way of opening energy gaps in electronic structures of solids is by creating periodic variations in electron density at atomic sites rather than at bond sites. This type of distortion is called a *charge density wave*, which can be either static, i.e., a frozen structural distortion, or dynamic, i.e., moves throughout the structure. An example of a 1-d CDW occurs in Wolfram's red salt  $[\text{Pt}(\text{NEtH}_2)_4\text{Br}]^{2+}(\text{Cl}^-)_2$ :



A qualitative description of the band structure for the undistorted chain can focus just on the important orbitals: the chain is built from square-planar  $[\text{Pt}(\text{NEtH}_2)_4]^{3+}$  units and  $\text{Br}^-$  ions to give octahedrally coordinated Pt sites. Therefore, the important orbital for Pt–Br interactions along the chain is the Pt  $5d_{z^2}$  AO, which is assigned 1 valence electron for  $\text{Pt}^{3+}$ . This band is Pt–Br  $\sigma$ -antibonding and acquires its dispersion because the bottom of the band, at the zone center, involves just Br 4s contributions, whereas the top of the band, at the zone boundary, involves just Br 4p

contributions. Now, this Pt  $5d_{z^2}$ -centered band is half-filled, and the structure is susceptible to a Peierls distortion. However, Pt–Br bond distance alternation will not affect the band structure, nor will it change the position of the Fermi level. All Pt centers remain equivalent with each other, so the qualitative band structure does not change. The distortion that does open an energy gap is  $[\text{Pt}(\text{NEtH}_2)_4\text{Br}_2]^{2+}[\text{Pt}(\text{NEtH}_2)_4]^{2+}$ , in which each  $\text{Pt}^{3+}$  site *disproportionates* into a  $\text{Pt}^{4+}$  site and a  $\text{Pt}^{2+}$  site.  $\text{Pt}^{4+}$  is  $d^6$ , which favors locally octahedral coordination by shifting the 2 surrounding Br atoms closer to this site. On the other hand,  $\text{Pt}^{2+}$  is  $d^8$ , which favors locally square-planar coordination as the 2 Br ligands shift away from this site. In the solid, this distortion is *static* with alternating  $\text{Pt}^{4+}$  and  $\text{Pt}^{2+}$  sites that opens an energy gap near the Fermi level. The  $5d_{z^2}$  AO at the Pt site with the shorter Pt–Br distances goes up in energy as the *antibonding* interaction increases. The  $5d_{z^2}$  AO at the Pt site with the longer Pt–Br distances goes down in energy as the *antibonding* interaction decreases. As a result, 1 electron goes from one Pt site to the other.

**(47) 2-d Graphene –  $\pi$ -Bands:** Tight-binding electronic structure calculations are typically carried out according to the following steps:

- Identify the basis set of atomic orbitals within the unit cell and construct Bloch functions for each one.
- Construct the Hamiltonian matrix for a wavevector  $\mathbf{k}$  in the irreducible wedge of the first Brillouin zone using the Bloch functions from part (a).
- Diagonalize the Hamiltonian matrix to obtain  $E_{\mathbf{k}}$  and wavefunctions  $\psi_{\mathbf{k}}$ , which are expressed as linear combinations of the atomic orbitals.
- Repeat steps (b) and (c) for different values of  $\mathbf{k}$  in and on the boundaries of the irreducible wedge of the Brillouin zone.
- Analyze the total spectrum of energy levels to obtain band structures ( $E_{\mathbf{k}}$  vs.  $\mathbf{k}$  plots), DOS and COOP/COHP curves to understand chemical bonding and electronic structure.

As an example of applying this procedure, consider the  $\pi$ -bands of the hexagonal planar net of graphene. In the unit cell, there are two C  $2p_z$  AOs, labeled “1” and “2”, and each atom has 3 nearest neighbors: atom “1” with 3 atom “2” neighbors and atom “2” with 3 atom “1” neighbors. The irreducible wedge of the Brillouin zone is the triangle determined by the three points:  $\Gamma = (0,0)$ ;  $K = (\frac{1}{3}, \frac{1}{3})$ ; and  $M = (\frac{1}{2}, 0)$ . The coordinates of the  $\mathbf{k}$ -points are given with respect to the two reciprocal lattice vectors  $\mathbf{a}_1^*$  and  $\mathbf{a}_2^*$ . Following the procedure outlined above, the Bloch functions for each basis function are:

$$\varphi_{1\mathbf{k}}(x, y) = \frac{1}{\sqrt{N}} \sum_{m,n} e^{2\pi i(k_1 m + k_2 n)} \varphi_1(x - m, y - n) \quad \text{and} \quad \varphi_{2\mathbf{k}}(x, y) = \frac{1}{\sqrt{N}} \sum_{m,n} e^{2\pi i(k_1 m + k_2 n)} \varphi_2(x - m, y - n).$$

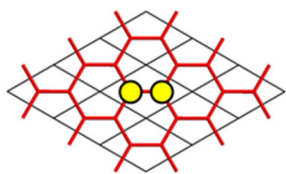
The coordinates of the functions are given in fractional coordinates with respect to the lattice constants of graphene. The  $2 \times 2$  Hamiltonian matrix using Hückel theory, which includes just nearest neighbor interactions, is:

$$H(k_1, k_2) = \begin{pmatrix} \alpha & \beta + \beta e^{2\pi i k_1} + \beta e^{-2\pi i k_2} \\ \beta + \beta e^{-2\pi i k_1} + \beta e^{2\pi i k_2} & \alpha \end{pmatrix}.$$

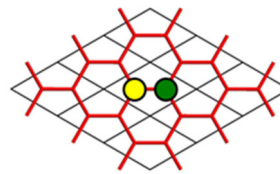
Diagonalizing this matrix leads to the eigenvalues (band energies):

$$E(k_1, k_2) = \alpha \pm \beta [3 + 2 \cos 2\pi k_1 + 2 \cos 2\pi k_2 + 2 \cos 2\pi(k_1 + k_2)]^{1/2},$$

and the eigenfunctions, which are Bloch functions using the two basis functions formed by the bonding and antibonding combinations of  $2p_z$  AOs within the unit cell:



$$\pi_{\mathbf{k}}(0,0) = \frac{1}{\sqrt{2}}(\varphi_1 + \varphi_2)$$



$$\pi_{\mathbf{k}}^*(0,0) = \frac{1}{\sqrt{2}}(\varphi_1 - \varphi_2)$$

Using Bloch's theorem, the corresponding crystal orbitals in any unit cell are:

$$\pi_{\mathbf{k}}(m,n) = e^{2\pi i(k_1 m + k_2 n)} \pi_{\mathbf{k}}(0,0) \quad \text{and} \quad \pi_{\mathbf{k}}^*(m,n) = e^{2\pi i(k_1 m + k_2 n)} \pi_{\mathbf{k}}^*(0,0).$$

The analytical equation for  $E(k_1, k_2)$  can be used to plot the energy band diagram along special lines of the Brillouin zone:  $\Gamma$ - $\Gamma$ ;  $\Gamma$ - $K$ ; and  $K$ - $M$ ; which creates a cycle around the boundary of the irreducible wedge. For each wavevector, there are two eigenvalues. In general, no analytical expression exists, so that these curves are computed by selecting a grid of points along each direction. The DOS and COOP curves are evaluated using numerous  $\mathbf{k}$ -points selected from a grid in and on the boundary of the irreducible wedge. The DOS and COOP curves are symmetrical about the energy value  $\alpha$  = energy of the C  $2p_z$  AO. Since each valence AO has 1 electron, the Fermi level from graphene is  $\alpha$ . States below  $\alpha$  are  $\pi$ -bonding; states above  $\alpha$  are  $\pi$ -antibonding. The DOS curve goes to zero at the Fermi level. As a result, 2-d graphene is called a "zero-gap semiconductor". In the band structure, the origin of this effect are the two bands that seemingly cross each other at the wavevector  $K$ . Indeed, energy values at wavevectors just surrounding the point  $K$  form two cones whose tips meet exactly. These are called *Dirac cones* and they impart special transport properties to the electrons in graphene. To understand how the Dirac cones arise in graphene, let's examine the crystal orbitals using symmetry arguments.

**(48)** Since the Dirac cones occur around the wavevector  $K$ , we'll examine wavefunctions along the direction  $\Gamma$ - $K$ - $M$ :

$\Gamma$ -point (0,0): There is no phase change from one unit cell to another:

$$\pi_{\Gamma}(m,n) = e^{2\pi i(0m+0n)} \pi_{\Gamma}(0,0) = \pi_{\Gamma}(0,0); \quad E(\pi_{\Gamma}) = \alpha + 3\beta.$$

$$\pi_{\Gamma}^*(m,n) = e^{2\pi i(0m+0n)} \pi_{\Gamma}^*(0,0) = \pi_{\Gamma}^*(0,0); \quad E(\pi_{\Gamma}^*) = \alpha - 3\beta.$$

The  $\pi$ -bonding band is totally bonding; the  $\pi$ -antibonding band is totally antibonding. As a result, the energies are the lower and higher extremes of the  $\pi$ -band structure.

Moving toward the wavevector  $K$ , recall that directions in reciprocal space correspond exactly with directions in real space. From the structure of graphene, this direction has reflection symmetry, and the  $\pi$ -bonding orbital  $\pi_{\mathbf{k}}(0,0)$  is *symmetric*, whereas the  $\pi$ -antibonding orbital  $\pi_{\mathbf{k}}^*(0,0)$  is *antisymmetric*. Furthermore, we can continue along the line  $\Gamma$ - $K$  and intersect the  $\mathbf{k}$ -point  $(\frac{1}{2}, \frac{1}{2})$ , which is another  $M$ -point of reciprocal space. The advantage of using this point rather than  $(\frac{1}{2}, 0)$  is that the crystal orbitals at this different  $M$ -point will retain their symmetric/antisymmetric relationships with the reflection symmetry. Therefore,

$M$ -point  $(\frac{1}{2}, \frac{1}{2})$ : There are phase changes for translations involving odd numbers of steps along  $\mathbf{a}_1$  and  $\mathbf{a}_2$ :

$$\pi_{\mathbf{M}}(m,n) = e^{2\pi i(\frac{1}{2}m + \frac{1}{2}n)} \pi_{\mathbf{M}}(0,0) = (-1)^m (-1)^n \pi_{\mathbf{M}}(0,0); \quad E(\pi_{\mathbf{M}}) = \alpha - \beta.$$

$$\pi_{\mathbf{M}}^*(m,n) = e^{2\pi i(\frac{1}{2}m + \frac{1}{2}n)} \pi_{\mathbf{M}}^*(0,0) = (-1)^m (-1)^n \pi_{\mathbf{M}}^*(0,0); \quad E(\pi_{\mathbf{M}}^*) = \alpha + \beta.$$

The crystal orbital derived from the  $\pi$ -bonding  $\pi_{\mathbf{k}}(0,0)$  orbital becomes slightly antibonding because of the phase changes in adjacent unit cells. Likewise, the crystal orbital derived from the  $\pi$ -antibonding  $\pi_{\mathbf{k}}^*(0,0)$  orbital becomes slightly bonding. Therefore, the two energy bands cross each other because they have different symmetry characteristics with respect to the reflection plane. It turns out that they cross at the wavevector  $\mathbf{K}$ .

$\mathbf{K}$ -point ( $1/3, 1/3$ ): The analysis for this point is somewhat complicated because the two wavefunctions are degenerate:

$$\pi_{\mathbf{K}}(m, n) = e^{2\pi i(\frac{1}{3}m + \frac{1}{3}n)} \pi_{\mathbf{K}}(0,0) = \left[ \cos \frac{2\pi(m+n)}{3} + i \sin \frac{2\pi(m+n)}{3} \right] \pi_{\mathbf{K}}(0,0); E(\pi_{\mathbf{K}}) = \alpha.$$

$$\pi_{\mathbf{K}}^*(m, n) = e^{2\pi i(\frac{1}{3}m + \frac{1}{3}n)} \pi_{\mathbf{K}}^*(0,0) = \left[ \cos \frac{2\pi(m+n)}{3} + i \sin \frac{2\pi(m+n)}{3} \right] \pi_{\mathbf{K}}^*(0,0); E(\pi_{\mathbf{K}}^*) = \alpha.$$

Since these two wavefunctions are degenerate and orthogonal to each other, any linear combinations will remain proper eigenfunctions of the Hamiltonian. Therefore, forming  $(\pi_{\mathbf{K}} + \pi_{\mathbf{K}}^*)$  and  $(\pi_{\mathbf{K}} - \pi_{\mathbf{K}}^*)$  creates two new wavefunctions. The in-phase combination has nonzero coefficients only at atom “1” sites; the anti-phase combination has nonzero coefficients only at atom “2” sites. In this way, these two wavefunctions reveal themselves to be nonbonding orbitals.

In summary, the structural symmetry allows certain band crossings to occur and the number of valence electrons sets the Fermi level so that graphene takes advantage of the Dirac cones.

**(49)** An alternative approach to performing electronic structure calculations on extended, crystalline solids using the unit cell and constructing Bloch functions is to build large fragments of the extended structure. For the group of translations, each  $\mathbf{k}$ -point is a different irreducible representation, and the number of  $\mathbf{k}$ -points counts the number of unit cells in the structure as determined by the periodic boundary conditions. For a large number of unit cells, the corresponding real space calculation requires a large assembly of atoms. In a comparison of the  $\pi$ -MOs of various fragments of graphene with the DOS curve for graphene, the DOS pattern emerges for the  $C_{54}$  fragment, although the results are limited by the termination of the structure. In fact, these MO diagrams may be appropriate for interpreting certain nanoscale phenomena.

**(50)** A complete calculation of the electronic structure of graphene uses the valence AOs of carbon, which include  $2s, 2p_x, 2p_y, 2p_z$ . In a DFT-based calculation, a 3-d structure must be used, but the distance between adjacent graphene-type planes can be set quite large so that any interlayer interactions are negligible. Depending on the calculation type, the intervening region may be filled with functions but no nuclei.

The band structure is certainly more complex than the simple model discussed above because there are 8 basis functions in the unit cell. Nevertheless, since the nodal plane of the  $2p_z$  AO is the plane of the atomic structure of graphene, the  $\pi$ -bands are distinctive and cross the  $\sigma$ -bands formed by the  $2s, 2p_x, 2p_y$  AOs. In fact, the dispersion from the DFT calculation is reproduced quite nicely by the simple Hückel calculation because symmetry controls much of these results. The bottom of the  $\pi$ -band at the  $\Gamma$ -point drops below the top of the  $\sigma$ -bonding bands derived exclusively from the  $2p_x, 2p_y$  AOs. Below the Fermi level, there are 3  $\sigma$ -bonding bands. Although we can consider  $sp^2$  hybrid orbitals at each C atom, the actual electronic structure has these wavefunctions dispersed over a broad energy range of  $\sim 15$  eV at  $\Gamma$  between the  $2s$  and the

degenerate  $2p_x, 2p_y$  crystal orbitals. The DOS curve illustrates a near-zero DOS at the Fermi level and the sharp peaks slightly above and below this energy. The C–C COOP curve indicates optimized orbital interactions for graphene because all bonding states are occupied, and antibonding states are unoccupied.

The electronic structure of graphene will be disrupted significantly when interactions between the planar layers becomes significant, as occurs for graphite. These interactions will affect the  $\pi$ -bands more than the  $\sigma$ -bands because the lobes of the  $2p_z$  AOs point toward adjacent planes. Features of the DOS curve near the Fermi level of graphene will change and become non-zero, so that graphite is a poor metal.